Nanostructure and Mechanical Measurement of Highly Oriented Lamellae of Melt-Drawn HDPE by Scanning Probe Microscopy

Binyang Du, Jian Zhang, Qingling Zhang, Decai Yang, and Tianbai He*

State Key Laboratory of Polymer Physics and Chemistry, Changchun Institute of Applied Chemistry, Chinese Academy of Sciences, Changchun, Jilin, 130022, China

Ophelia K. C. Tsui

Department of Physics, Hong Kong University of Sciences & Technology, Clear Water Bay, Kowloon, Hong Kong

Received May 30, 2000; Revised Manuscript Received July 24, 2000

ABSTRACT: Scanning probe microscopy was used to *simultaneously* determine the molecular chain structure and intrinsic mechanical properties, including anisotropic elastic modulus and friction, for lamellae of highly oriented high-density polyethylene (HDPE) obtained by the melt-drawn method. The molecular-scale image of the highly oriented lamellae by friction force microscopy (FFM) clearly shows that the molecular chains are aligned parallel to the drawing direction, and the periodicities along and perpendicular to the drawing direction are 0.26 and 0.50 nm, respectively. The results indicate that the exposed planes of the lamellae resulting from the melt-drawn method are (200), which is consistent with results of transmission electron microscopy and electron diffraction. Because of the high degree of anisotropy in the sample, coming from alignment of the molecular chains along the drawing direction, the measured friction force, F, determined by FFM is strongly dependent on the angle, θ, between the scanning direction and the chain axis. The force increases as θ is increased from 0° (i.e., parallel to the chain axis) to 90° (i.e., perpendicular to the chain axis). The structural anisotropy was also found to strongly influence the measurements of the transverse chain modulus of the polymer by the nanoindentation technique. The measured value of 13.8 GPa with transverse modulus was larger than the value 4.3 GPa determined by wide-angle X-ray diffraction, which we attributed to anisotropic deformation of the lamellae during nanoindentation measurements that was not accounted for by the elastic treatment we adopted from Oliver and Pharr. The present approach using scanning probe microscopy has the advantage that direct correlations between the nanostructure, nanotribology, and nanomechanical properties of oriented samples can be determined simultaneously and simply.

Introduction

Polymers are used in a variety of engineering applications nowadays. For a large number of these applications, the mechanical properties dictate a polymer's suitability for the intended usage. In the past, the isotropically averaged parameters would be sufficient for the consideration, even when the polymer is anisotropic as the domain size of an ordered polymer is usually ~μm. However, as engineering applications are approaching nanometer scales, anisotropy in the physical properties will have to be considered. Traditional methods used to determine the mechanical properties of polymers, such as tensile testing techniques, are macroscopic and provide an average measurement due to contributions of many molecular chains with random orientations. To determine the intrinsic mechanical properties of ordered polymer chains along different directions, such as chain modulus along and perpendicular to the chain axis, indirect probes such as laser Raman spectroscopy,[1] elastic neutron scattering,[2] and wide-angle X-ray diffraction[3] have been used. A main disadvantage of these techniques is the complex and tedious calculations that must be carried out to deal with the data. The major difficulty preventing the direct mechanical approach from being usable comes from the lack of samples with well-organized structures that are big enough for studies with conventional mechanical testing methods.

With the invention of scanning probe microscopy (SPM),[4] it is now possible to make characterization of surface morphology, mechanical, and other physical properties from ~10^2 μm down to ~1 nm over a broad range of fundamental and applied science.[5,6] For instance, SPM has been used to observe the nanostructures of polymer single crystals[7,8] and to measure the nanomechanical properties, such as hardness,[9] elasticity,[10] and viscoelasticity,[11,12] of polymer thin films. In this work, we used SPM to study the mechanical properties of polymer chains in a single domain within an oriented high-density polyethylene lamellae by direct mechanical means. By simultaneously recording the morphology of the polymer, a more precise structure−property relationship can be obtained. Briefly, highly oriented lamellae of high-density polyethylene with chain axis parallel to the supporting substrate were obtained by the melt-drawn method. The morphology and nanostructure of the highly oriented lamellae were observed by transmission electron microscopy (TEM) and SPM. Then the anisotropic friction and transverse elastic modulus (perpendicular to the polyethylene chain axis) were measured by friction force microscopy (FFM) and nanoindentation, respectively, while the longitudinal elastic modulus (along the chain axis) of polyethylene is already known from a previous study by us.[13] On the basis of the structure of the highly oriented lamellae,

* To whom correspondence should be addressed. E-mail: tbhe@ns.ciac.ac.cn.

10.1021/ma000943g CCC: $19.00
Published on Web 09/07/2000

we shall discuss the anisotropy we found in the mechanical properties measured.

Experimental Section

Sample Preparation. The high-density polyethylene (HDPE) utilized in this work is Marlex 6003 with a weight-average molecular weight of 2×10^5 Da. Highly oriented thin films of HDPE with lamellar structure were prepared according to the method by Petermann and Gohil[14] using very high longitudinal flow rate on the order of 10^4 s^{-1}. A solution of HDPE in xylene (0.5 wt %) was uniformly spread on a preheated glass plate, and the solvent was allowed to evaporate at the preset temperature (128 °C). A thin supercooled polyethylene film was then quickly drawn vertically from the melt. The drawing speed was 4 cm s^{-1}. This procedure yields films that are 50 to 100 nm thick. A small piece would then be taken out from the film and put onto a copper grid if it was to be studied by TEM but would be put onto a freshly cleaved mica if it was to be investigated by SPM. Before TEM or SPM studies, the thin films were annealed in a vacuum oven at 128 °C for 2 h.

Instrumentation. The morphology of the films were observed by a JEOL 2010 TEM with an accelerating voltage 200 kV. The thin films were shadowed by Pt for better contrast. A gold sample was used for the calibration of the electron diffraction (ED) spacing.

The nanostructure and friction properties of the lamellae were investigated using FFM with a silicon nitride tipped cantilever of spring constant 0.06 N/m[15] (Digital Instruments). Imaging was carried out in constant force mode.

The elastic modulus of polyethylene chains perpendicular to the chain axis was measured by nanoindentation on the highly oriented lamellae prepared as described above. Nanoindentation was performed using a Digital Instruments Multimode NanoScope IIIa SPM with a diamond tip mounted on a stainless steel cantilever from the same manufacturer. The diamond tip is a Berkovich-like three-sided pyramid with an apex angle of about 60°, yielding an included half-angle α of about 21.6°[16] (manufacturer's specification). The nominal spring constant of the stainless steel cantilever is 186 N/m, and the angle of the cantilever to the horizontal was 12°. The cantilever sensitivity was measured using a sapphire sample before and after the indentation. For all SPM indentation studies, the indentation rate was 4 Hz and the lateral compensation angle was 25°. These values for the indentation rate and lateral compensation angle were optimized using methods detailed in refs 13 and 17.

Data Analysis of the Nanoindentation. Before nanoindentation measurements, the sample was imaged using the "tapping mode" to locate the area of interest. During nanoindentation measurements, the probe oscillates as it is lowered onto the surface in a manner similar to the last stage of the tip engagement process. When the probe detects the sample surface, the probe oscillation was stopped and the indentation process was "triggered", and a force−distance curve was acquired. The indented sample was then imaged again using "tapping mode" for comparison with the image taken before nanoindentation. During indentation, the cantilever is driven down toward the sample surface by a piezoelectric actuator, resulting in both probe tip deflection and sample indentation. The amount of sample indentation is dependent on the relative stiffness of the sample and the cantilever probe. In the extreme case where the sample is infinitely stiff compared to the probe tip, no indentation will occur. The relationship between the displacement of the piezoelectric actuator (Δz_p), the tip deflection (Δz_t), and sample indentation, i.e., surface deformation of the sample (Δz_s), is simply[18,19]

$$\Delta z_s = \Delta z_p - \Delta z_t \cos(12°) \tag{1}$$

where the cos(12°) factor corrects for the fact that the cantilever has a built-in 12° inclination to the horizontal. The indentation force applied to the sample, P, can be obtained directly from $P = k_c \Delta z_t \cos(12°)$, where k_c is the spring constant of the cantilever. In the force−distance curves measured by us, the ordinate is the indentation force, P, and the abscissa is the sample deformation, h (=Δz_s). A typical nanoindentation curve on the highly oriented lamellae of HDPE is shown in Figure 1, where h_f is the permanent deformation of the sample after complete unloading, h_{max} the maximum deformation at the peak indentation force P_{max}, and h_0 the contact depth that would be made in the sample if the indentor were a flat punch. (For conical indentors such as the one used in this experiment, the contact depth is $\sim 0.72 h_0$.[20]) We analyzed the load-deformation curves we acquired by the method Oliver and Pharr proposed,[20] in which the hardness impression of the sample produced by nanoindentation was considered. As pointed out by these authors, the effective elastic modulus E_{eff} of the sample is generally related to the stiffness of the sample at unloading, $S = dP/dh(h_{max})$, and the projected contact area at the maximum indentation, A: [20]

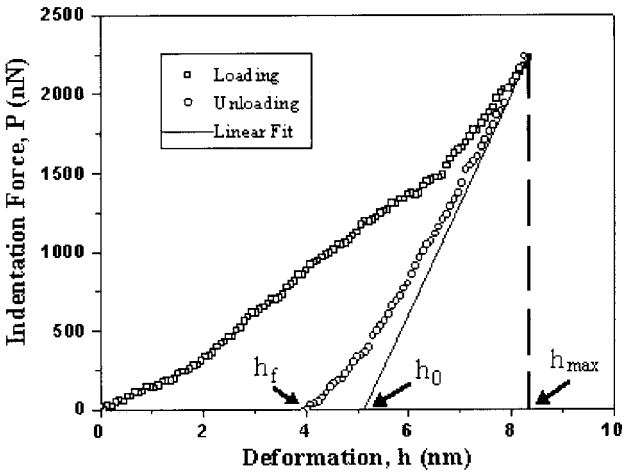

Figure 1. A typical nanoindentation curve on highly oriented lamellae of HDPE with ca. 2.3 μN. h_f is the permanent indentation depth of the contact impression after unloading, h_0 is the contact depth that would have been made by a flat indentor, and h_{max} is the maximum indentation depth at peak indentation force, P_{max}. The dotted line is the expected unloading curve of a flat indentor. The slope of the dotted line is equal to that of the unloading curve at P_{max}, which is the measured value of the sample stiffness, S.

$$E_{eff} = \frac{1}{\beta}\frac{\sqrt{\pi}}{2}\frac{S}{\sqrt{A}} \tag{2}$$

where β is a geometrical factor dependent on the shape of the indentor. For the Berkovich-like indentation tip used here, β is assumed as 1.034.[20] The effective modulus E_{eff} takes into account the elastic deformation occurring in both the sample and the indentation tip and is related to the Young's modulus of the sample, E_s, and that of the tip, E_t, by

$$\frac{1}{E_{eff}} = \frac{1-\nu_s^2}{E_s} + \frac{1-\nu_t^2}{E_t} \tag{3}$$

where ν_s and ν_t are the Poisson's ratio of the sample and the tip, respectively. In this work, a diamond tip was used; hence, $E_t = 1141$ GPa and $\nu_t = 0.07$.

It has been reported that the roundness of the indentation tip might have influence over the resultant nanoindentation measurements. Assuming a perfect indentation tip will result in an underestimation for the projected contact area and hence an overestimate of the elastic modulus for the sample (see eq 2). Since the tip used in this work is not perfectly sharp, the influence of roundness of the tip on the projected contact area should be considered. Sawa et al.[21] calculated a correction for the projected contact area, A, to account for the effect of roundness of a tip. For a three-sided pyramidal indentation

tip used in the present study, the corrected A by Sawa et al. is given by

$$A = 3\sqrt{3}(\tan^2\alpha)(h_0 + \Delta h_T)^2 \quad (4)$$

where the correction factor Δh_T is

$$\Delta h_T = (R/8)\cot^2\alpha \quad (5)$$

Here, R and α are respectively the tip radius and the half-including angle of the three-sided pyramidal indentation tip. The tip radius, R, and correction factor, Δh_T, can be deduced from indentation measurements on a standard sample of fused silica using eqs 2−5 (Valley Design Corp. Westford, MA). It is used because it is elastically isotropic, its modulus of 72 GPa is well-known, and its modulus is independent of the indentation depth.[20]) On the basis of five indentation measurements on a fused silica sample, we found that the tip radius, R, and the correction factor, Δh_T, were 45 ± 5 nm and 36 ± 4 nm, respectively.

The unloading stiffness, $S = dP/dh$ at $h = h_{max}$, i.e., the initial slope of the unloading curve, can be determined from the empirically found relation for the indentation−deformation curve:

$$P = B(h - h_f)^m \quad (6)$$

where B and m are fitting parameters. Combining eqs 2−6, the Young's modulus of the sample, E_s, can be determined from the indentation−deformation curve by

$$E_s = \frac{(1 - \nu_s^2)S}{1.053(h_0 + 36) - 0.001S} \quad \text{(in GPa)} \quad (7)$$

Results and Discussion

Morphology of Highly Oriented Lamellae. Figure 2 shows a typical bright field TEM micrograph obtained from the melt-drawn HDPE films, in which the crystalline regions appear dark and the amorphous regions appear bright. The arrow indicates the film drawing direction. As seen, our sample is consisting of highly oriented lamellar crystals with growth direction perpendicular to the film drawing direction and lamellar longitudinal length ranging from a few tenths of nanometers to a few micrometers, consistent with previous results.[22] The average thickness of the lamellae is about 36 nm. According to the electron diffraction pattern of the same sample (inset of Figure 2), the lamellar crystals display a (200) surface plane texture with the c axis, i.e., the chain axis, parallel to the drawing direction and the a axis perpendicular to the plane of film. This uniplanar texture is likely a result of the oriented nucleation in the thin film with the preference in PE to have the b axis as the fast growth direction.[22]

To examine the (200) surface plane texture of the highly oriented lamellae further, FFM is employed. The morphological features of corrugated surfaces can sometimes be enhanced in FFM images since the torsion signal contains the derivative information on the surface topography.[8] In Figure 3a is shown the FFM topographical image of the melt-drawn HDPE thin film. The arrow indicates the drawing direction. The highly oriented crystalline lamellae are clearly evident, with the fast growth direction being perpendicular to the drawing direction. The average thickness of the lamellae measured by FFM is about 48 nm, which is ∼30% larger than the value found by TEM mentioned above. We believe that this is because in FFM, the tip cannot distinguish the amorphous regions from the lamellae. Hence, the lamellar thickness 48 nm obtained by FFM indeed corresponds to the period of the oriented lamellae, which includes both the amorphous and the crystalline regions. To obtain a molecular-scale FFM image of the lamellae, a smaller area in the crystalline region in Figure 3a (5.27 nm × 5.27 nm) was selectively scanned. The main panel of Figure 3b displays the resultant image, where 2D fast Fourier transformation filtering

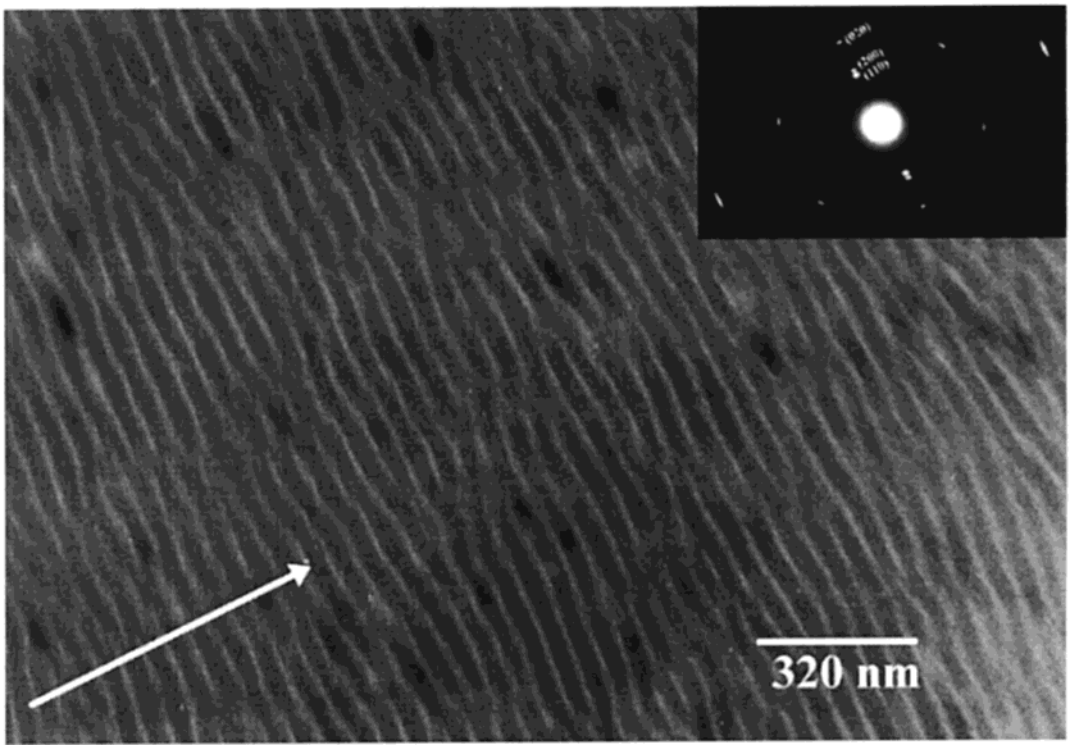

Figure 2. TEM image of a melt-drawn HDPE film. The electron diffraction pattern is shown in the inset. The arrow indicates the drawing direction.

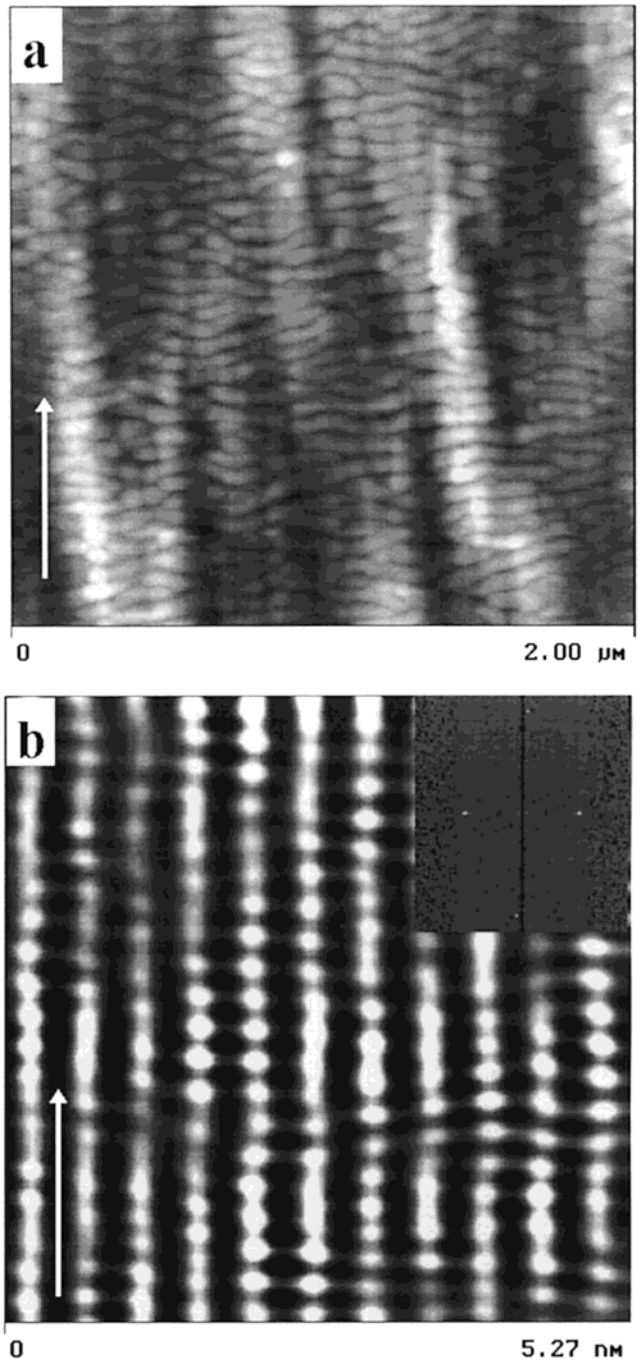

Figure 3. (a) Topographical FFM image of a melt-drawn HDPE film, which clearly reveals that the film consists of highly oriented lamellae with the fast growth direction perpendicular to the draw direction shown by the arrow. The *Z* range is 150 nm. (b) Molecular-scale FFM image of the highly oriented lamellae is shown in (a). The *Z* range is 0.03 V. The scan rate was set as 17.4 Hz to minimize noise. The 2D fast Fourier spectrum is given in the inset. The arrow indicates the drawing direction.

had been performed to remove the high-frequency noise. The scan rate was chosen to be 17.4 Hz to minimize the amount of noise produced in the image. The arrow in the figure indicates the drawing direction. Consistent with results depicted above, molecular chains of the lamellae are oriented along the drawing direction. The inset of Figure 3b shows the 2D fast Fourier spectrum for the image shown in the main panel. Four intense diffraction spots could be clearly seen, based on which the spectral periodicity along and perpendicular to the drawing direction are determined as 0.26 and 0.50 nm, respectively. As is well-known, the identity periodicity of the zigzag molecular chain ($-CH_2-$ units) of HDPE is 0.253 nm. The orthorhombic unit cell parameters of HDPE crystals are 0.742, 0.495, and 0.253 nm along the *a*, *b*, and *c* axis, respectively. From the above TEM and ED results, the sample displays a (200) surface plane texture of the lamellae, with the *c* and *b* axes being along and perpendicular to the drawing direction, respectively. In a (200) plane of HDPE, we expect the distance between two neighboring chains to be 0.495 nm, i.e., the periodicity along the *b* axis. Accordingly, we may identify the spectral periodicity of 0.50 nm perpendicular to the draw direction in the molecular-scale FFM image (Figure 3b) with the distance between two neighboring chains and the spectral periodicity of 0.26 nm along the draw direction in the same image with the identity periodicity of the zigzag molecular chains of HDPE. Therefore, all our TEM, ED, and FFM results are consistent with the conclusion that the exposed plane of the highly oriented HDPE lamellae is (200), with the chain axis being parallel to the drawing direction.

Anisotropic Friction Property of Highly Oriented Lamellae. When a tip scans over the surface of a sample in FFM, deformation in the sample surface occurs because of mechanical interactions between the tip and the surface, giving rise to the necessity of a minimum work to initiate or sustain tip scanning. This critical work accounts for the friction force between the tip and the surface. To monitor friction forces in this work, the line direction was set to retrace for the recording of FFM images. In this scheme, bright regions correspond to small friction forces and dark regions to high friction forces in the resultant images.[14]

As the above results show, the melt-drawn HDPE films consist of highly oriented lamellae, with (200) exposed planes and high degree of molecular chain alignment in the lamellar surface. It is interesting to investigate how the friction property of this sample may depend, if it does, on the scanning angle, θ, between the scanning direction of the FFM tip and the chain axis. Shown in Figure 4a−d are the friction images of the sample at scanning angles 90°, 60°, 30°, and 0°, respectively. (The topographical image can be found in Figure 3a.) The arrow indicates the drawing direction (|| to the *c* axis). Evidently, the friction image gets brighter (lower friction) as the scanning angle is decreased from 90° to 0°. Therefore, the friction force, which acts on the FFM tip as it traverses the surface of the highly oriented lamellae, decreases as the tip scanning direction is increasingly aligned with the chains.

To quantitatively determine the friction force, friction hysteresis loops are acquired. Basically, the slow scan axis of FFM is first disabled, and then the tip is scanned back and forth repeatedly along the same path on the surface of the sample. Figure 5 shows the data obtained this way at different scanning angles. The friction force is determined by halving the difference between the line-averaged lateral forces along each scanning direction in the friction loop. The fact that the shapes of the forward and backward leg of the hysteresis loop look alike indicates that the friction force is independent of the scanning direction. However, there is an offset between the two, which reveals the amount of dissipation in mechanical energy. We further note that there is no observable change in the shape of the hysteresis

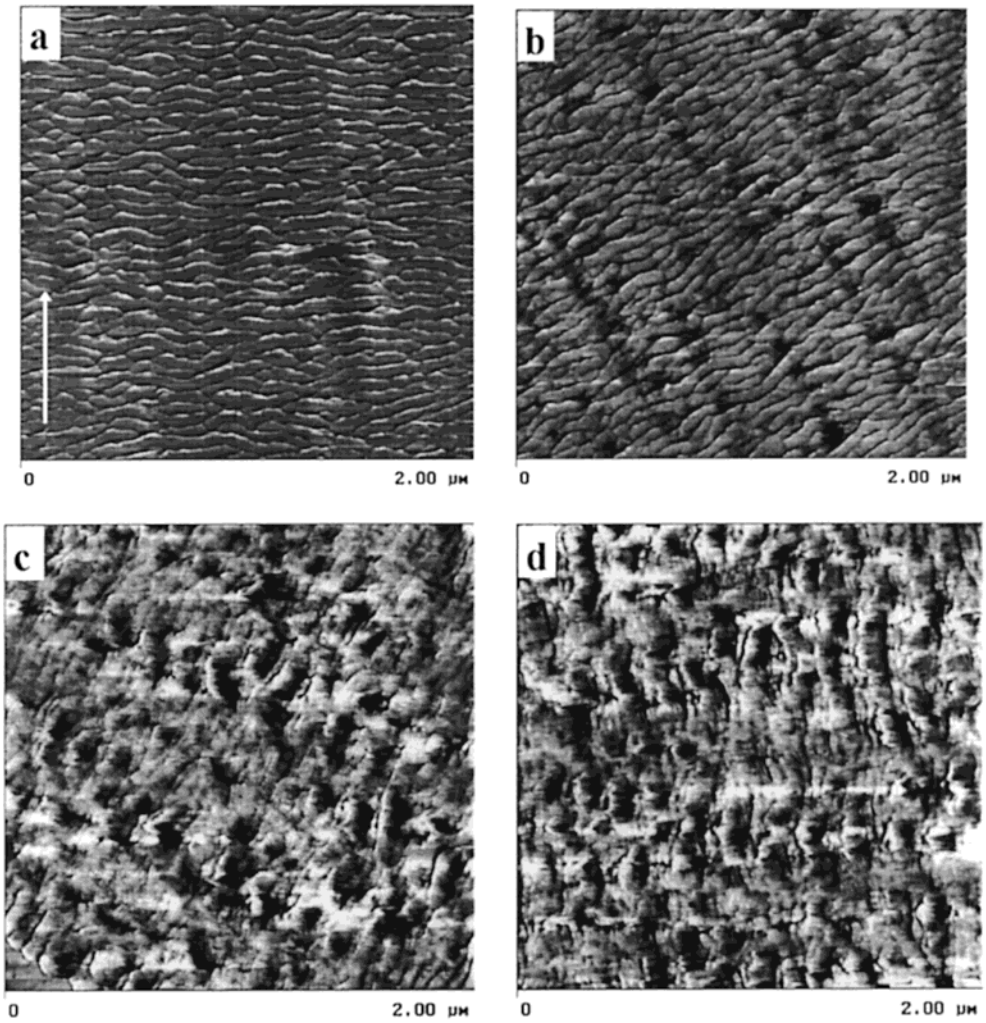

Figure 4. FFM images of highly oriented lamellae (the same sample used in Figure 3a) with various scanning angles, θ, of (a) 90°, (b) 60°, (c) 30°, and (d) 0°. The *Z* range is 0.2 V. The scanning angle is the angle between the scanning direction of the FFM tip and the chain axis (*c* axis) of highly oriented lamellae. The arrow in (a) indicates the drawing direction. The line direction of the FFM was set as retrace (right to left) for recording the images in the present experiments.

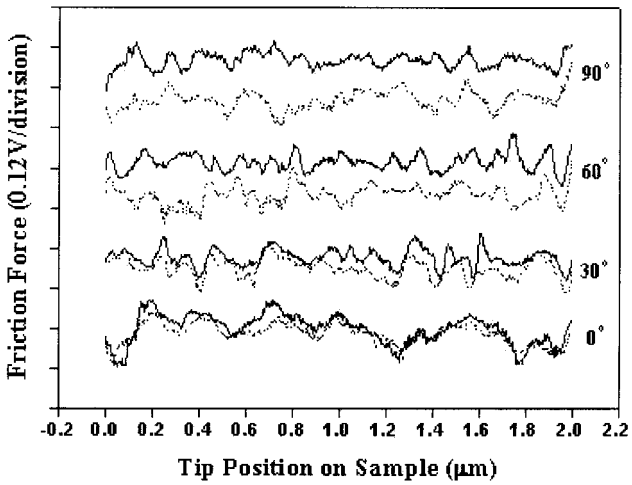

Figure 5. Tip−surface friction force on highly oriented lamellae as the sample is moved back and forth along the same line on the sample. Four sequential loops of friction versus position with scanning angles of 90°, 60°, 30°, and 0° are shown, offset vertically with respect to one another. The solid lines represent the left-to-right scans, and the dashed lines, the right-to-left scans.

loops obtained in consecutive scans (not shown). This suggests that the sample is not damaged during the course of tip scanning; hence, variations in the friction curve truly reflect the local variation in the friction of the sample. The friction forces of the sample normalized to the value measured at $\theta = 0°$ are plotted versus the scanning angle, θ, in Figure 6 (open squares), which quantitatively shows the anisotropy in the friction of the lamellae. As seen, the highest friction force between the tip and the lamellae occurs when the scanning angle is 90°. In other words, the friction is the highest when the tip is scanning perpendicular to the chain axis. As mentioned above, the lamellae are consisting of parallel arrays of polymer chains lying along the *c* axis, each containing molecular units ($-CH_2-$) that are arranged in a zigzag manner along the length of the chain. When the tip scans perpendicular to the chain axis, i.e., $\theta = 90°$, the tip will necessarily bump into the chains and likely produce acoustic excitations by which dissipation occurs. When the tip scans along the chain axis, i.e., $\theta = 0°$, on the other hand, molecular-scale position shifting of the tip may occur during scanning to avoid crossing the chains, which causes dissipations. This may allow for a smaller friction force. When θ is between 0° and 90°, consider the friction force as composed of two parts: one perpendicular to the chain axis and one parallel to the chain axis. If the two parts combine simply like independent vector components, one will ex-

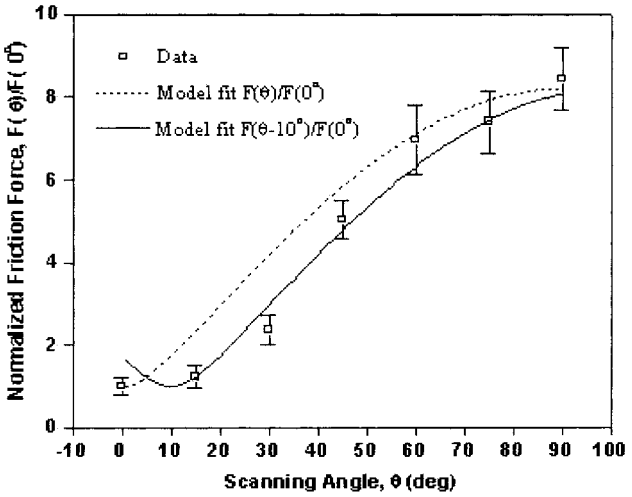

Figure 6. Relationship between the friction force normalized to the value measured at 0° and the scanning angle, which indicates that the friction force increased as the angle between the chain axes and the scanning direction increased from 0° to 90°.

pect the normalized friction, $F(\theta)/F(0)$, to be $\sqrt{\{\cos^2\theta + [F(90°)/F(0)]^2 \sin^2\theta\}}$. This expression is plotted as dashed line in Figure 6, with $F(90°)/F(0) = 8.2$ being used. Clearly, this simple model overestimates the friction force for $\theta < \sim 60°$. Probably, small adjustments of the tip position occur continually, during scanning, to lower dissipation. This will naturally happen if the tip shifts toward a direction with scanning angle $<\theta$. However, this shift in the direction will have to be corrected when the torsion in the tip can no longer be sustained by the friction force of the sample, and slippage of the tip back to the imposed scanning direction θ will occur. This forseeable zigzag behavior in the friction force during the course of scanning seems evident in all friciton hysteresis loops displayed in Figure 5. Assuming that for the majority of the time the tip samples the lower friction force of the smaller scanning angle $= (\theta - 10°)$, the measured average friction force will then be closer to $F(\theta - 10°)$. The solid line in Figure 6 shows the model form for $F(\theta - 10°)/F(0)$, which clearly demonstrates excellent agreement with the data. The interpretation for the anisotropic friction measurements based on the simple picture proposed here seems to work quite well. A word needs to be said about the accuracy in the measurement of θ since an error of 10° in θ may also explain the data. However, an inspection on the relative orientations of the lamellae in the FFM images of Figure 4a,b (where the relative bearing is nominally 30°) showed that the accuracy in θ is much better than 10°.

Chain Modulus of Highly Oriented Lamellae. In the above section, it is clearly shown that anisotropy in the structure of the oriented lamellae causes the measured friction to depend on the scanning direction. In this section, we shall examine how the mechanical properties may differ along and perpendicular to the chain axis of the lamellae. Previously we carried out direct measurements of the longitudinal elastic modulus (along the chain axis) on single crystals of polyethylene with the chain axis perpendicular to the supporting substrate using the nanoindentation technique.[13] For the polyethylene samples examined in the present work, the chain axis of the oriented lamellae is parallel to the supporting substrate; therefore, these samples are suitable for direct measurements of the transverse elastic modulus (perpendicular to the chain axis). In the following, the transverse elastic modulus of oriented polyethylene will be measured by nanoindentation and be related to the structure of the lamellae.

Table 1. Elastic Modulus Measured by Nanoindentation on Highly Oriented Lamellae with Indentation Forces of 1.1, 1.7, 2.3, and 4.5 μN

P_{max} (μN)	h_f (nm)	h_{max} (nm)	h_f/h_{max}	E_s (GPa)
1.1	2.0 ± 0.2	4.7 ± 0.2	0.43	14.1 ± 1.9
1.7	2.9 ± 0.2	6.1 ± 0.2	0.48	13.8 ± 1.6
2.3	3.8 ± 0.4	8.4 ± 0.5	0.45	13.5 ± 1.9
4.5	7.4 ± 0.4	13.2 ± 0.2	0.56	17.2 ± 0.4

It has been reported that when the indentation depth exceeds 10−25% of the thickness of the sample, the effect of the substrate on nanoindentation measurements should be considered.[23] Since the thickness of the HDPE thin films we prepared for nanoindentation measurements is 50−100 nm, the appropriate indentation depth should be in the range 5−10 nm. The typical indentation force of our instrument ranges from 1 to 100 μN with a resolution of 0.5 μN.[16] Three indentation forces, P, of 1.1, 1.7, and 2.3 μN were selected for the present indentation studies. For example, for the indentation curve shown in Figure 1, P was 2.3 μN, and the maximum indentation depth (h_{max}) was ca. 8.4 nm with a permanent indentation depth (h_f) of ca. 3.8 nm. On the other hand, the ratio h_f/h_{max} determines how accurately one can determine the elastic modulus of a sample using the Oliver−Pharr method.[24] It was found that when h_f/h_{max} is < 0.7, the measured value by the Oliver−Pharr method matches well with that obtained from the finite element analyses. But when h_f/h_{max} is >0.7, the Oliver−Pharr method will lead to large errors.[24] With the three values of P stated above, the h_f/h_{max} ratios were about 0.4−0.5 (Table 1). Therefore, the Oliver−Pharr method (eq 7) was used in the present study to evaluate the transverse elastic modulus, E_s, of highly oriented HDPE. The values we obtained for E_s of the sample based on 10 measurements at three different indentation forces are shown in Table 1, where the Possion's ratio of polyethylene has been assumed to be 0.41.[25] As seen in Table 1, the values of E_s determined by nanoindentation, 13.8 GPa, agree with one another but are ∼3 times larger than 4.3 GPa measured by wide-angle X-ray diffraction.[3] In highly oriented lamellae, the chain axis of polyethylene is parallel to the film surface. Thus, when indentation takes place in the sample, the elastic displacements are primarily transverse to the chains. However, since the formation of the hardness impression produced by the tip on the sample surface involves deformation in all directions, it is foreseeable that the measured modulus will be an average quantity due to elastic modulus along all directions. The chain modulus along the chain axis is about 240 GPa for polyethylene.[3] Using the result determined by wide-angle X-ray diffraction, namely 4.3 GPa for the transverse elastic modulus, the elastic anisotropy in the material is 56. Such a large value of anisotropy may explain the substantial enhancement in E_s found here by the nanoindentation technique. Clearly, modifications to the analysis to incorporate effects of elastic anisotropy on the elastic modulus measurement by indentation methods are needed for reliable quantitative measurements.

A further point of interest from Table 1 is that, for the lowest three indentation forces used, the measured

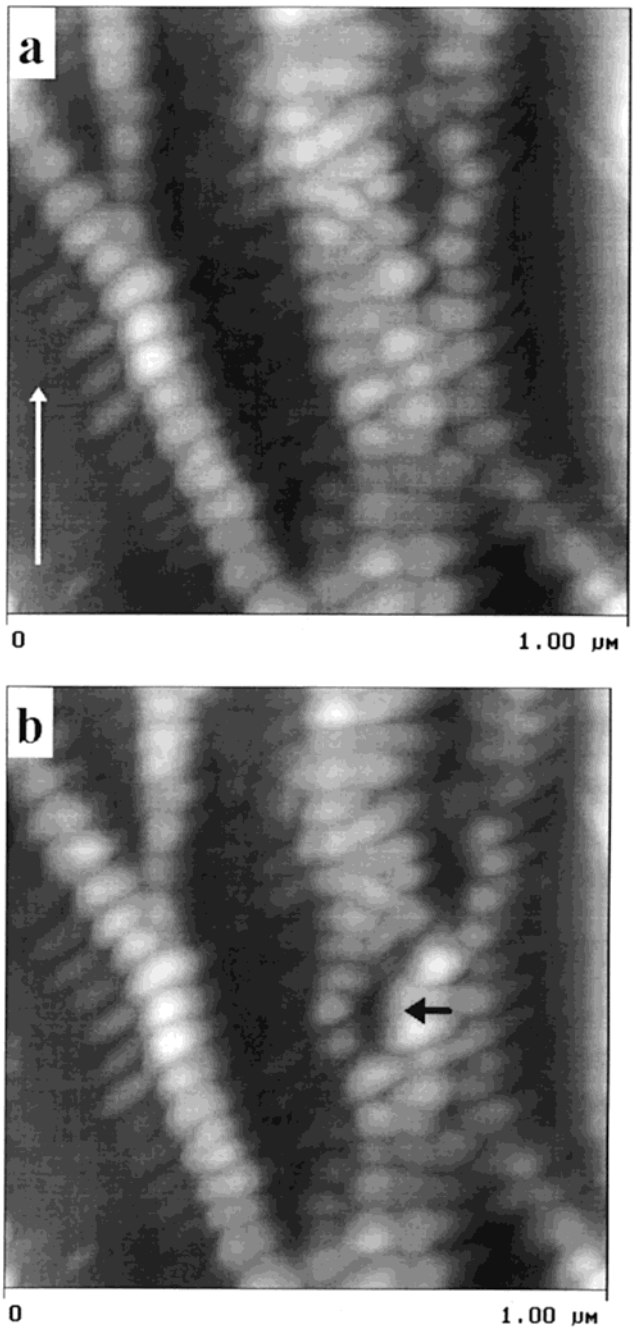

Figure 7. Topographical SPM images of highly oriented lamellae of HDPE (a) before and (b) after indentation with indentation force of ca. 4.5 μN. The Z range is 150 nm. The arrow indicates the drawing direction. The arrow in (b) points at the impression produced by the indentation of the tip into the lamellae.

values of E_s agree within experimental uncertainties. This shows that these measurements were acquired in the linear response regime of the sample. The measured E_s becomes substantially larger (~25% increment) when the maximum load was increased to 4.5 μN. To investigate this observation, we examined the morphology of the sample before and after the application of the (P_{max} = 4.5 μN) indentation force by SPM (Figure 7, a and b, respectively). The images clearly show that the indentation did occur within areas where the lamellae were found. This excludes the possibility that the measurements may be due to the amorphous region. We further note that the indentation depth is ca. 13.2 nm (see Table 1). This is more than 10−25% of the sample

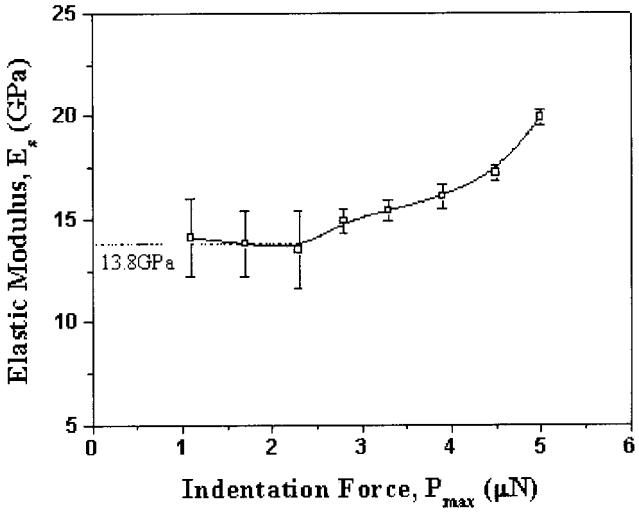

Figure 8. Relationship between the elastic modulus E_s and the indentation force P_{max} on a highly oriented film of HDPE.

thickness. As mentioned above, the mechanical response of the hard substrate will also contribute to the mechanical response of the lamellae. Furthermore, a large indentation will necessarily include a larger portion of the elastic response along the chain direction. Hence, an increase in the measured elastic modulus is reasonable. To further confirm the enhancement in E_s observed, we repeated the measurements at values of P_{max} from 1.1 μN up to 5.0 μN. The results are shown in Figure 8. As seen, the elastic modulus appears to plateau near an indentation force of 2.3 μN, being relatively constant at 13.8 GPa below this indentation force, within experimental uncertainties. The enhancement in the measured E_s from P_{max} = 2.3 μN up to 5.0 μN indeed signifies the onset of a growing contribution of the elastic anisotropy to the mechanical response of the sample with increasing indentation load. Studies on films with different thicknesses are currently under way to determine whether the increases shown in Figure 8 at large indentation forces come from the effect of the substrate or the exaggerated influence of the longitudinal chain modulus.

Conclusions

Scanning probe microscopy was used to characterize, simultaneously, the nanostructure and the mechanical properties of highly oriented lamellae of HDPE obtained by the melt-draw method. The molecular-scale FFM image of a lamellar surface clearly shows that the molecular chains in lamellae are aligned parallel to the drawing direction. The periodicities along and perpendicular to the drawing direction are 0.26 and 0.50 nm, respectively, corresponding to the lattice parameters in the (200) plane of the oriented lamellae of HDPE. These dimensions are consistent with measurements obtained independently by transmission electron microscopy and electron diffraction. Besides the microstructure, friction force microscopy was also able to observe the anisotropy in the friction force of the highly oriented HDPE film. The friction force increased as the scanning angle was increased from 0° (parallel to the chain axis) to 90° (perpendicular to the chain axis). The transverse elastic modulus, E_s, of HDPE was determined, using the nanoindentation technique. E_s was 13.8 GPa, which was substantially larger than the value (4.3 GPa) obtained by wide-angle X-ray diffraction. We attribute the dif-

ference to contributions from the (higher) anisotropic stiffness along all other directions to the sample deformation that occurred during nanoindentation. Our results show that while it is convenient to use the indentation technique to measure an elastic modulus of a material, the anisotropy in the material, if substantial, may interfere with the measurements.

Acknowledgment. This work was supported by the National Science Foundation of China and subsidized by the Special Funds for the Major State Basic Research Projects of China. O.K.C.T. acknowledges support by the Polymer Physics Laboratory, Changchun Institute of Applied Chemistry, under Project R120001W and Hong Kong University of Science and Technology through the Research Grant Council of Hong Kong under Project DAG98/99.SC24. The sapphire sample for calibrating the detection sensitivity of SPM was kindly supplied by Drs. S. Mogonov and L. Huang of Digital Instruments (Veeco Instruments Incorporated).

References and Notes

(1) Shaufflele, R. F.; Shimanouchi, T. *J. Chem. Phys.* **1967**, *47*, 3605−3610.
(2) Capaccio, G.; Ward, I. M. *Polym. Eng. Sci.* **1975**, *15*, 219−224.
(3) Sakurada, I.; Ito T.; Nakamae, K. *J. Polym. Sci.* **1966**, *C15*, 75−91.
(4) Binng, G.; Quate, C. F.; Gerber, C. *Phys. Rev. Lett.* **1986**, *56*, 930−933.
(5) Magonov, S. N.; Reneker, D. H. *Annu. Rev. Mater. Sci.* **1997**, *27*, 175−222.
(6) Radmacher, M.; Tillmann, R. W.; Fritz, M.; Gaub, H. E. *Science* **1992**, *257*, 1900−1905.
(7) Patil, R.; Reneker, D. H. *Polymer* **1994**, *35*, 1909−1914.
(8) Motomatsu, M.; Nie, H.-Y.; Mizutani, W.; Tohumato, H. *Polymer* **1996**, *37*, 183−185.
(9) Drechsler, D.; Karbach, A.; Fuchs, H. *Appl. Phys. A* **1998**, *66*, S825−S829.
(10) Domke, J.; Radmacher, M. *Langmuir* **1998**, *14*, 3320−3325.
(11) Tanaka, K.; Takahara, A.; Kajiyama, T. *Macromolecules* **1998**, *31*, 863−869.
(12) Tsui, O. K. C.; Wang, X. P.; Ho, J. Y. L.; Ng, T. K.; Xiao, X. *Macromolecules* **2000**, *33*, 4198−4204.
(13) Du, B.; Liu, J.; Zhang, Q.; He, T. *Polymer*, in press.
(14) Petermann, J.; Gohil, R. M. *J. Mater. Sci.* **1979**, *14*, 2260−2264.
(15) Digital Instruments Inc., NanoScope III[a], MultiMode Scanning Probe Microscope Instruction Manual, Santa Barbara, CA, 1997.
(16) Digital Instruments Inc., Support Note No. 225, Rev. F, Santa Barbara, CA, 1998.
(17) VanLandingham, M. R. *Microsc. Today* **1997**, *97−10*, 12−15.
(18) VanLandingham, M. R.; Mcknight, S. H.; Palmese, G. R.; Elings, J. R.; Huang, X.; Bogetti, T. A.; Eduljee, R. F.; Gillespie, J. W. Jr. J. *Adhesion* **1997**, *64*, 31−59.
(19) Nie, H. Y.; Motomastu, M.; Mizutani, W.; Tokumoto, H. *Thin Solid Films* **1996**, *273*, 143−148.
(20) Oliver, W. C.; Pharr, G. M. *J. Mater. Res.* **1992**, *7*, 1564−1583.
(21) Sawa, T.; Akiyama, Y.; Shimamoto, A.; Kohichi, T. *J. Mater. Res.* **1999**, *14*, 2228−2232.
(22) Yang, D. C.; Thomas, E. L. *J. Mater. Sci.* **1984**, *19*, 2098−2110.
(23) Pharr, G. M.; Oliver, W. C. *MRS Bull.* **1992**, *17*, 28−33.
(24) Bolshakov, A.; Pharr, G. M. *J. Mater. Res.* **1998**, *13*, 1049−1058.
(25) Choy, C. L.; Leung, W. P. *J. Appl. Polym. Sci.* **1986**, *32*, 5883−5901.

MA000943G